Materials Science and Engineering A 399 (2005) 134–140

MATERIALS SCIENCE & ENGINEERING A

www.elsevier.com/locate/msea

Measurement and modeling of room temperature co-deformation in WC–10 wt.% Co

V. Livescu [a,*], B. Clausen [a], J.W. Paggett [b], A.D. Krawitz [b], E.F. Drake [c], M.A.M. Bourke [a]

[a] *MST-8/LANSCE, Los Alamos National Laboratory, Los Alamos, NM 87545, USA*
[b] *Department of Mechanical and Aerospace Engineering, University of Missouri, Columbia, MO 65211, USA*
[c] *REEDHycalog™/Grant Prideco, Houston, TX 77252, USA*

Abstract

In situ neutron diffraction measurements were performed on a tungsten carbide (WC)–10 wt.% cobalt (Co) cemented carbide composite subjected to compressive loading. The sample was subjected to consecutive load/unload cycles to −500, −1000, −2000 and −2100 MPa. Thermal residual stresses measured before loading reflected large hydrostatic tensile stresses in the binder phase and compressive stresses in the carbide phase. The carbide phase behaved elastically at all but the highest load levels, whereas plasticity was present in the binder phase from values of applied stress as low as −500 MPa. A finite element simulation utilizing an interpenetrating microstructure model showed remarkable agreement with the complex mean phase strain response during the loading cycles despite its under-prediction of thermal residual strains.

Keywords: Cemented carbide composites; Neutron diffraction; Residual strain; In situ co-deformation; FE modeling; Thermal residual stresses

1. Introduction

WC–Co cemented carbide composites have been used for many years for rock drilling and cutting tool applications. Previous neutron diffraction work in this field concentrated on aspects relating to the residual stress state: effects of sintering and fabrication on the residual stresses [1], internal strain and relative stresses of WC and Co as a function of temperature [2], progressive binder deformation response over the composition range of binder metastability [3]. However, questions related to the sharing of loading between the two phases remain unanswered.

This study observed the load sharing characteristics for the carbide (WC) and binder (Co) phases in the cemented carbide composite. This included consideration of the thermal residual stresses (TRS) arising during cooling from the sintering temperature (1450 °C) due to a difference of a factor of two in coefficients of thermal expansion between WC (6 μm/m °C) and Co (12.8 μm/m °C) [4]. Diffraction enables the strain response in each phase to be determined as a function of physical and crystallographic direction. In principle either X-rays or neutrons could be used but, due to their limited penetration (in the presence of tungsten) and the influence of surface condition, X-rays cannot be used to study bulk stress effects. Conversely [5], the penetration depth for neutrons is sufficient to give a volume average result of approximately 1 cm^3.

2. Sample and loading history

The subject of this study was WC–10 wt.% Co (16 vol.%), material fabricated and metallurgically characterized by ReedHycalog™. The microstructure is shown in Fig. 1. Literature values for the modulus of elasticity are in the range of 572 [6] and 579 GPa [7]. The WC powder, with an average particle size of 1–2 μm, was used as a stress-free reference standard for the thermal residual strain measurements. The neutron measurements were performed on a cylindrical sample 12 mm in diameter and 28 mm in length. During the in situ loading the load was increased incrementally to maxima of

* Corresponding author.
E-mail address: vlivescu@lanl.gov (V. Livescu).

0921-5093/$ – see front matter © 2005 Elsevier B.V. All rights reserved.
doi:10.1016/j.msea.2005.02.024

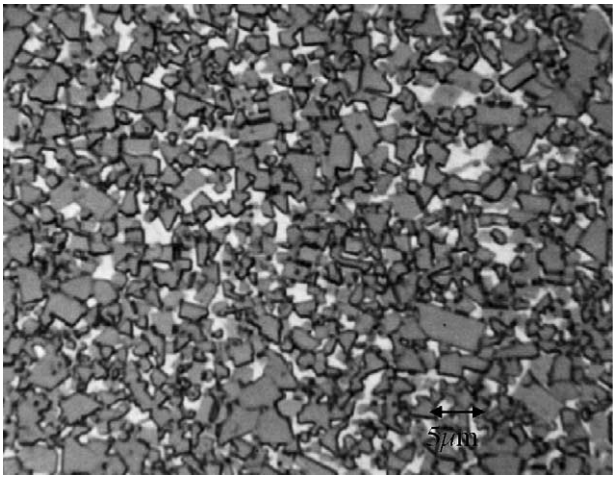

Fig. 1. Micrograph of WC–10 wt.% Co.

−500, −1000, −2000 and −2100 MPa with intervening unloads after each. Measurements were made under load control at the plateaus illustrated in Fig. 2. The macroscopic strains were monitored with a clip-gage extensometer.

3. Neutron diffraction experiment

The use of neutron diffraction for residual strain and for in situ loading has been widely reported ([2,8–12]). The initial TRS values were determined on the Missouri University Residual Stress Instrument (MURSI) at the University of Missouri Research Reactor. The WC 201 peak was used for the measurements; the wavelength employed, 1.6549 Å, placed the WC 201 peak at $2\theta \approx 92^\circ$. A small internal gauge volume was used to minimize peak shift due to differences in absorption between the samples and the WC powder used as a stress-free reference.

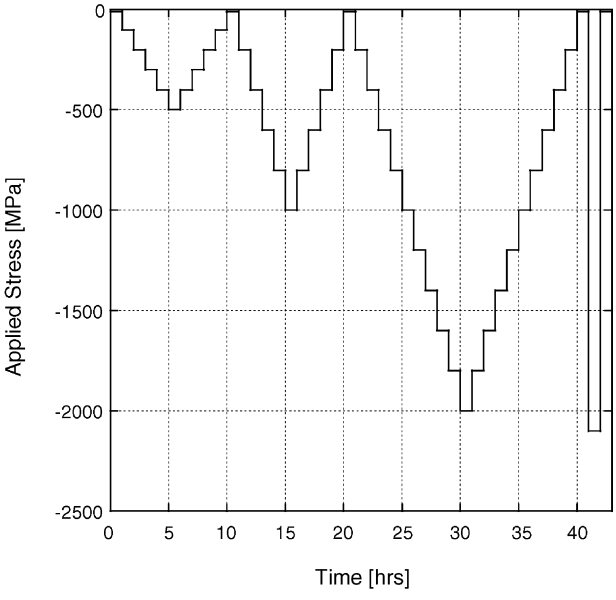

Fig. 2. Loading profile time history.

The strain was calculated from the peak positions of the sample and stress-free reference by

$$\varepsilon = \frac{\sin\theta_0}{\sin\theta} - 1, \tag{1}$$

where ε is the strain, θ_0 is the position of the stress-free reference peak and θ is the position of the peak from the sample. From the strain, the residual stress in the WC is calculated using Hooke's Law:

$$\sigma = \frac{E}{1-2\upsilon}\varepsilon, \tag{2}$$

where σ is the stress, E is Young's modulus and υ is Poisson's ratio. The value of E used for the WC 201 planes was 672 GPa and the value of υ was 0.25. These values are the directionally dependent crystallographic values calculated from the full elastic constant tensor given by Lee and Gilmore [13] and differ slightly from the macroscopic values used for the FE calculation (Table 3).

For the measurements under uniaxial compression we used the Spectrometer for Materials Research at Temperature and Stress (SMARTS), which was designed for structural materials studies [14] at the spallation neutron source at the Los Alamos Neutron Science Center (LANSCE). The sample loading axis was oriented at 45° to the incident beam and data was recorded simultaneously parallel and perpendicular to the uniaxial load by using the ±90° detector banks. The count time was 50 min for each stress level. Measurements at a pulsed neutron source are typically performed polychromatically and a complete diffraction pattern is recorded in each measurement (Fig. 3). The data is typically analyzed both by performing single peak fits and by performing Rietveld refinements. Provided there is no evidence of gross microstructural anisotropy from the single peak fits it is common practice to use strains calculated from the lattice parameters (determined from Rietveld analyses) to report the mean phase strain response of composite constituents, i.e. the WC and Co in this case. Thus, for the data reported below we report strains calculated from changes in the lattice parameters. In the case of WC we present the strain as $(2a + c)/3$ after Krawitz et al. [15,16]. A discussion of the single peak fit responses, which were qualitatively similar to the Rietveld responses, will be reported in a later publication. The 201 reflection used for residual strain measurements on MURSI

Table 1
Thermal residual strains and stresses in WC (measured on MURSI) and Co (inferred by force balance)

WC	
ε (με)	−303 ± 37
σ (MPa)	−407 ± 50
Co	
ε (με)	3747
σ (MPa)	2061

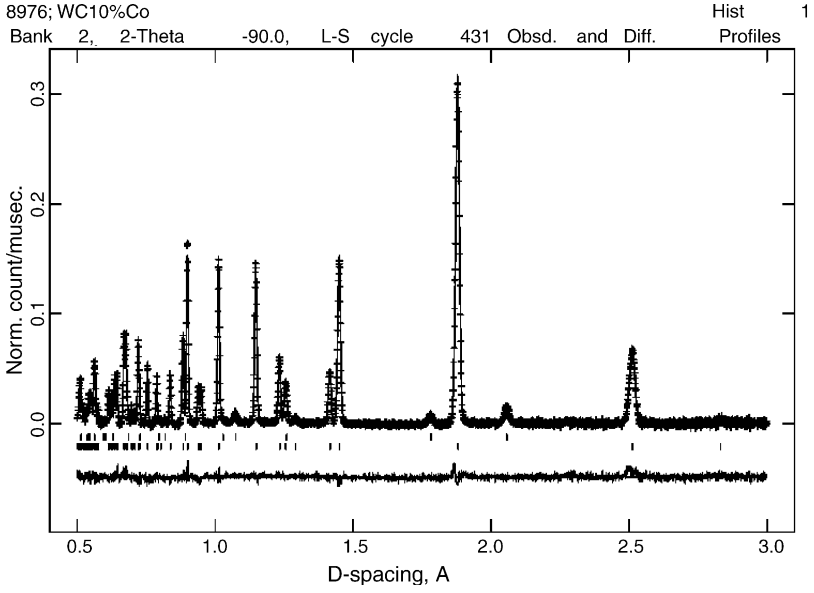

Fig. 3. Neutron diffraction spectrum.

showed a response close to the $(2a + c)/3$ average. Note that the strains reported for the in situ loading are reported relative to the initial strain state at the start of the test and thus are not absolute.

4. Results

4.1. Experimental results

The sample length measured before and after loading to a maximum of −2100 MPa reflected a permanent plastic deformation of less than 0.1%. Although the extensometer exhibited poor accuracy in the low range because of experimental problems, the total plastic strain was consistent with measured values in literature reports, as was the load–strain response that reflected curvature for loads as low as −500 MPa (Fig. 4). The initial elastic modulus measured from the extensometer data was 571.2 GPa.

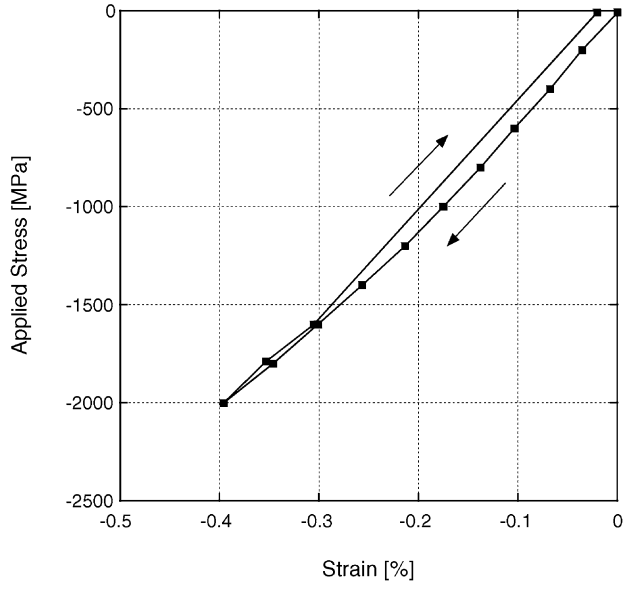

Fig. 4. Macroscopic stress–strain response to 2 GPa. Arrows show loading and unloading.

The initial thermal residual strains were determined for the WC prior to deformation by comparison with a sample of the unstressed powder. The stress was calculated using Hooke's law (E_{Co} = 209 GPa and E_{WC} = 672 GPa) and assumed that the diffraction-averaged stress state was hydrostatic since the measured strains are independent of sample orientation. Due to the low intensity of the Co peaks compared to the background, the thermal residual stress value of 2061 MPa and the corresponding strain value in the Co were inferred by force balance with the WC. The values are included in Table 1.

Strains were measured in situ under load. The evolution of the residual strains at each unload, i.e. after unload from −500, −1000, −2000 and −2100 MPa are reported in Table 2. Cobalt's small neutron scattering cross-section [17] renders it a poor neutron scatterer and as a consequence the

Table 2
Change in residual strain after unload from −500, −1000, −2000, −2100 MPa (Relative to initial unloaded strain state)

Pre-load (MPa)	Parallel to load		Perpendicular to load	
	WC ($\mu\varepsilon \pm 30$)	Co ($\mu\varepsilon \pm 130$)	WC ($\mu\varepsilon \pm 30$)	Co ($\mu\varepsilon \pm 130$)
−10	0	0	0	0
−500	−14	156	1	−21
−1000	−28	191	7	−64
−2000	31	487	109	−431
−2100	17	641	113	−501

Table 3
Material properties used for the FE simulation

Phase	Co	WC
Young's modulus (GPa)	209	680
Poisson's ratio	0.31	0.24
CTE (μm/m °C)	12.8×10^{-6}	6.0×10^{-6}

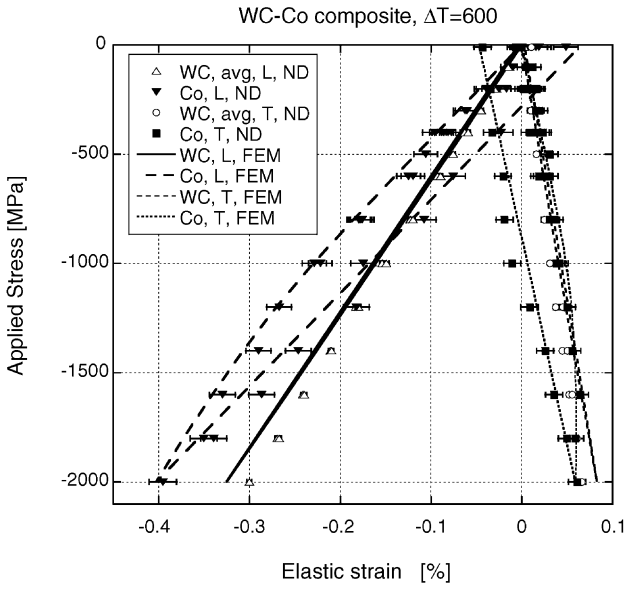

Fig. 5. Measured and calculated elastic phase strain responses. The average value for WC is calculated as $\varepsilon^E_{\text{avg}} = \frac{1}{3}(2\varepsilon^E_a + \varepsilon^E_c)$.

reported Co data is subject to relatively larger uncertainties than the WC data.

The evolution of the strains during the loading for the 0–2000 MPa ramp is shown in Fig. 5 together with the FE calculations.

4.2. Finite element model

The use of FE modeling to study mean phase strain response of composite systems has been applied to low volume fraction (10 or 20%) discrete particles in a ductile matrix (80–90%) such as AlTiC, AlSiC ([18,19]) and to interpenetrating microstructure problems such as BeAl [20] and to WC/Co [2]. In at least one case (the BeAl) the phase strain response of an interpenetrating microstructure was described with a simple mesh. In this study we evaluated several simple repeating array models' ability to predict the complex behavior described in Fig. 5 and in Table 1. With the thermal residual strain and the in situ loading values, the macroscopically determined modulus and a bound for the plastic strain (<0.1%) we have both macroscopic and microscopic information against which the model predictions can be compared.

The unit-cell model shown in Fig. 6 with material properties listed in Table 3 was ultimately chosen for its ability to describe the interpenetrating nature of the cemented carbide microstructure. The calculations were made using the ABAQUS [21] standard program, and the mesh was generated using second order 20 node brick elements with reduced integration points. To determine the thermal residual stresses in the composite, the cooling cycle from the sintering was included in the modeling. The temperature change in the cooling cycle was estimated to be 600 °C, based on the data presented in [22]. The WC was assumed to behave entirely elastically during the cooling and loading cycles. Information about the in situ yield and hardening behavior of the cobalt binder phase is limited, but we have estimated the yield stress to be 1050 MPa based on Vickers hardening data [23] and the rule-of-thumb that the yield stress is about three times the Vickers hardness. Other factors that increase the in situ yield are solution hardening due to W and C ([24,25]), the Hall–Petch effect (the average binder mean free path is 0.65 μm), and carbide constraint. Each of these factors is significant in WC–Co cemented carbides.

The material parameters for WC and Co used in the FEM calculations are given in Table 3. The von Mises yield stress of Co is set to −1050 MPa and a linear hardening of 9.5 GPa has been used to define the plastic behavior of the Co. The thermal residual strains were modeled using a ΔT of −600 °C and the coefficients of thermal expansion listed in Table 3.

4.3. Modeling results

The predicted mean thermal residual phase strain in the WC was −165.9 με, compared to the measured value of −303 με. In contrast, a similar FE model that has no interconnectivity between WC grains predicted only −105.6 με. This "cube in a cube" model represents a continuous binder in which WC "floats". Further, this model did not accurately predict the measured elastic strain response in the Co phase in the longitudinal and transverse directions, simultaneously.

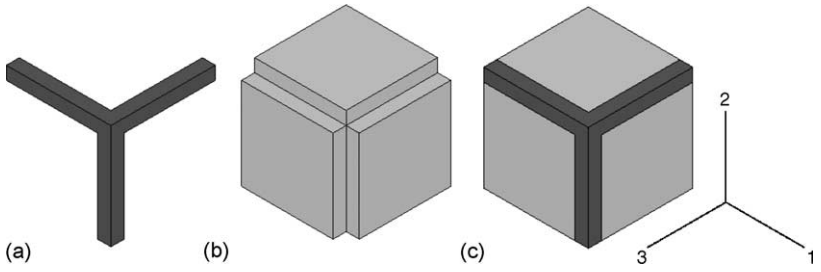

Fig. 6. FE model: (a) cobalt; (b) tungsten carbide; (c) FEM cell.

The "interpenetrating" model has continuity for both phases and approximates better the degree of constraint imposed by the WC phase on the Co phase. It appears more useful to speak of "WC constraint" rather than a "WC skeleton". The load-sharing characteristics and mechanical response as a function of composition will be discussed in future publications.

After the thermal residual strains were modeled the model was subjected to compressive loading cycles to mimic the in situ neutron diffraction load test and the results are shown in Fig. 5.

5. Comparison and discussion

A previous FE study [26] attempted to interpret diffraction peak broadening due to elastic strain distributions arising from cooling a composite or multiphase microstructure. The method involved averaging elastic strain output from a representative FE model to generate a strain distribution analogous to the averaging taking place in the diffraction process. Example applications were examined for thermal residual strain in WC–Ni composites with 11 and 60% Ni. The meshes used were based on actual microstructures. The stress in the WC, which is compressive on average, becomes tensile at corners and at locations that are normal to WC/Ni interfaces. The Ni stress, which is tensile on average, is compressive in narrow bands between WC particles. In addition, asymmetry of the Ni distribution on the high strain side, due to localized plastic flow, was successfully modeled for the 60 vol.% WC–Ni. This was a two-dimensional study that focused on the elastic strain distribution, not the mean thermal residual stress, and appeared to capture important aspects of the strain distribution. Also, no applied load was utilized. In the present case, we wanted to see if the mean phase response (on which the macroscopic response is based) could be predicted with a model that did not describe the detailed morphology of the microstructure.

The ability of the model to predict the thermal residual strain at the outset of the experiment is underestimated by almost a factor of two (-166 to $-303\,\mu\varepsilon$). Assuming that the material properties are correct then this disparity suggests that our simple model significantly underestimates the angularity in the microstructure (which acts to give stronger strain gradients and higher maxima). However, subject to the assumed material properties (Table 3), the agreement between model and experiment during the loading phase of the experiment is very good (Fig. 5). Note that ΔT was taken from [22] and that the only "free" parameters used in the model were the Co yield stress and the hardening behavior.

Although it is hard to resolve in Fig. 4, the stress-strain response shows curvature very early in the loading cycle, possibly as low as -500 MPa. We attribute this to the onset of localized binder plasticity [27] and it is consistent with the early development of the cobalt residual strain ($156\,\mu\varepsilon$ parallel to the loading direction after loading to -500 MPa) in Table 2. In the FEM calculations plasticity occurs in the cobalt phase during the cooling cycle, but only in very limited areas at the interface between the two phases (see Fig. 7b). This can be attributed to the stress concentrations due to the angularity of the mesh. The numerical value of these stresses and strains may vary if mesh size is changed, but as the affected volume is very small and limited to the interface, it does not significantly influence the volume average values that are used in the comparison with the measured data. The plastic zone generated during the cooling cycle does increase in size throughout the loading cycles, but very slowly until the applied stress exceeds approximately -1000 MPa. As a result, there is no true elastic loading of the composite as also shown experimentally [27]. The predicted modulus of 579.4 GPa matched the measured modulus of 571.2 GPa, indicating that the material properties in Table 3 are plausible. Clearly the value of the cobalt yield stress at -1050 MPa seems large but, as discussed above, there are reasons to believe that it is of this order. The choice of ΔT is an elastic approximation of the "set-up" process, i.e. the temperature dependence of available creep/plasticity mechanisms for inelastic accommodation of differential thermal strains.

We also explored the stress distributions and plastic strain history that are easily extracted from the model. We note, for example, that the mean phase stresses in the WC and Co, at

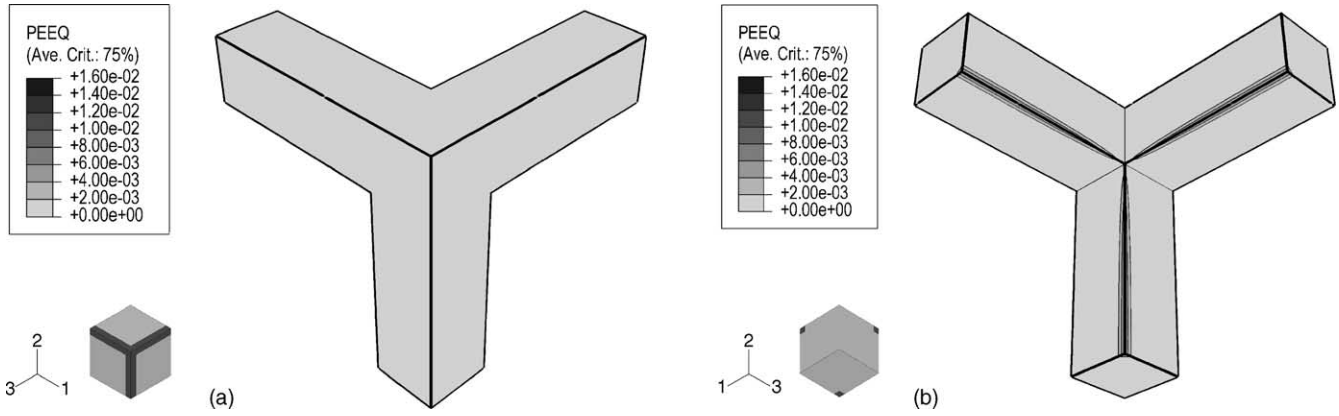

Fig. 7. Calculated equivalent plastic strains (PEEQ) in the cobalt binder after cool down. The cube next to the triad shows the orientation of the unit cell for the views.

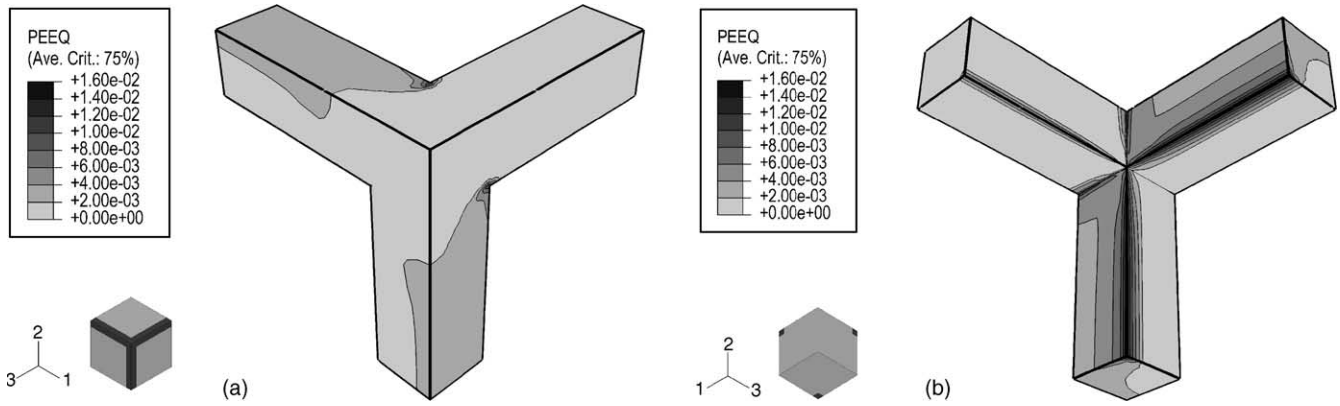

Fig. 8. Calculated equivalent plastic strains (PEEQ) in the cobalt binder at 2 GPa applied compressive stress. The cube next to the triad shows the orientation of the unit cell for the views.

−2100 MPa, are −2.29 and −1.05 GPa. However, the stress fields in the WC and Co are highly heterogeneous with a variation of at least 900 MPa in the von Mises stress across the bands of Co above and below the particles. Not surprisingly the lowest degree of plasticity is on the ligaments on the sides of the cobalt matrix parallel to the load.

From Figs. 7–10 it can be seen that the stress and strain state in the cobalt is very heterogeneous. The Co ligament parallel to the loading axis (axis 3 in Fig. 6) does not deform plastically upon loading as the applied load is in the opposite direction with respect to the thermal residual stresses. The two other ligaments (perpendicular to the loading axis)

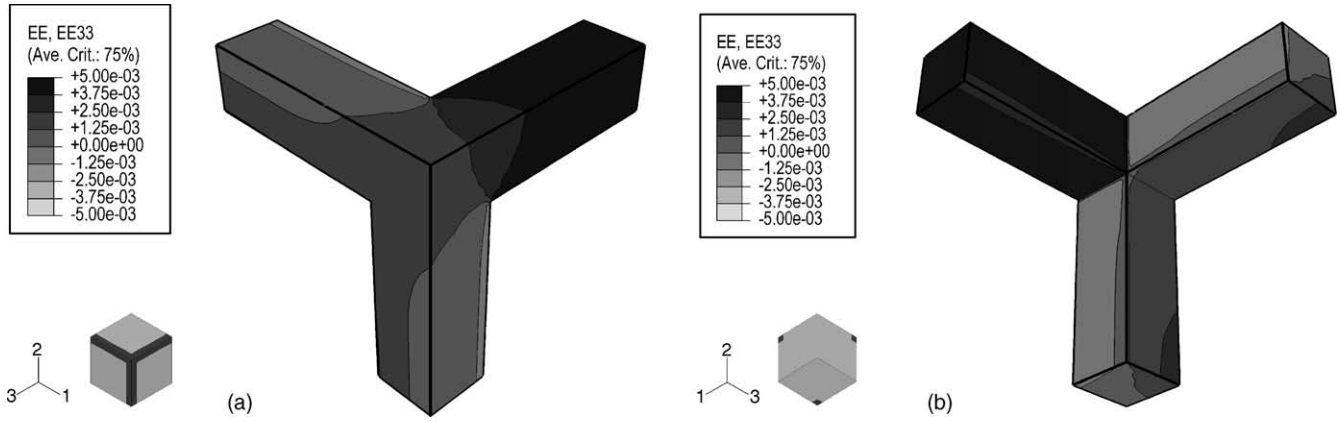

Fig. 9. Calculated elastic strains along the three axes (EE33) in the cobalt binder after cool down. The cube next to the triad shows the orientation of the unit cell for the views.

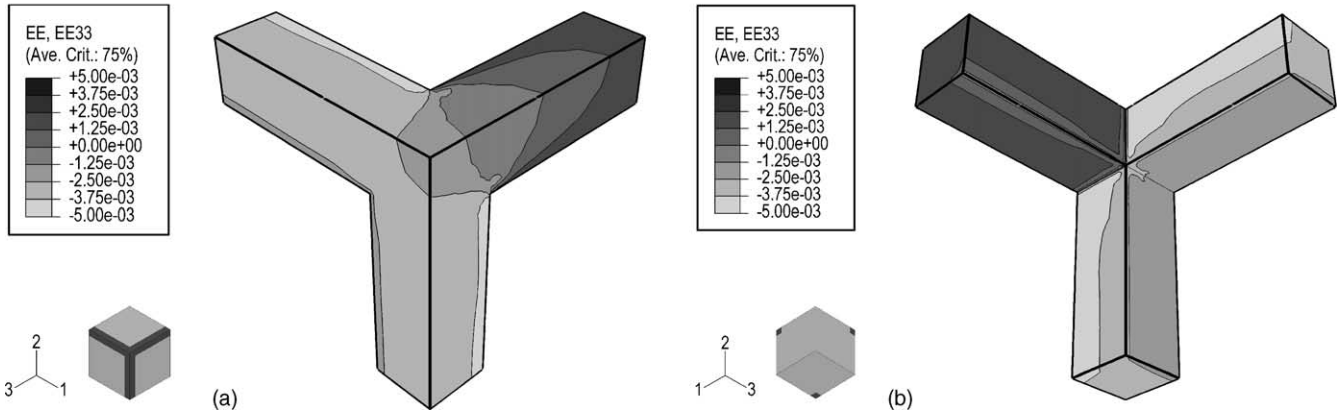

Fig. 10. Calculated elastic strains along the three axes (EE33) in the cobalt binder at 2 GPa applied compressive stress. The cube next to the triad shows the orientation of the unit cell for the views.

do deform plastically upon loading and therefore, they also show relatively higher von Mises stress levels. We know from previous work [28] that the residual stress relaxes anisotropically so that this data should prove important.

While the model appears too simple to predict accurately stress distributions in the composite, its agreement with the bulk response is remarkable. It represents the first 3D FEM work on a cemented carbide-like structure, incorporating both binder plasticity and strain hardening as well as considering both thermal and applied loading.

6. Conclusions

A neutron diffraction study of residual stress and phase strain response under load was performed on WC–10 wt.% Co. Changes in the macroscopic residual strains were noted after loading to −500 MPa indicating that inelasticity – presumably binder plasticity – occurs at such a low stress. Individual phase strain response under load was determined for both the WC phase and the Co phase. The carbide phase behaves elastically except when unloading from −2000 and −2100 MPa when tensile residual strains of approximately 100 $\mu\varepsilon$ are present in the transverse direction.

Measurement of thermal residual stress indicated a hydrostatic stress in the WC phase of −407 MPa that, according to force balance, corresponded to 2061 MPa in the Co phase.

An FE model comprised of a regular array of interpenetrating WC and Co under-predicted the thermal residual strains but provided close quantitative predictions of the mean phase strain response—subject only to reasonable yield stress and hardening behavior assumptions.

Further optimization of some parameters used in the FE simulation may provide additional utility from this simple model in approximating average deformation responses, i.e. thermal load, Co yield stress and hardening characteristics. However, more complex, realistic model geometries will be necessary to predict strain distribution responses of cemented carbides as well as extent to the extremes of contiguity.

Acknowledgements

We acknowledge the support of ReedHycalog™/Grant Prideco, through a grant to the University of Missouri. Funding for SMARTS and the operation of Lujan Center, a national user facility, was provided by the United States Department of Energy, Office of Basic Energy Sciences under contract W-7405-ENG-36.

References

[1] J.W. Paggett, E.F. Drake, A.D. Krawitz, R.A. Winholtz, N.D. Griffin, Int. J. Refractory Met. Hard Mater. 20 (2002) 187–194.
[2] D. Mari, A.D. Krawitz, J.W. Richardson, W. Benoit, Mater. Sci. Eng. A 209 (1996) 197–205.
[3] C.H. Vasel, A.D. Krawitz, E.F. Drake, E.A. Kenik, Metall. Trans. 16A (1985) 2309–2317.
[4] Y.S. Touloukian, Thermal Expansion: Metallic Elements and Alloys, IFI/Plenum Press, New York, 1975.
[5] A.D. Krawitz, Mater. Sci. Eng. 75 (1985) 29–36.
[6] P. Schwartzkopf, R. Kieffer, Cemented Carbides, Macmillan, New York, 1960, p. 139.
[7] T. Lin, M. Hood, G.A. Cooper, J. Am. Ceram. Soc. 77 (1994) 1562–1568.
[8] M.A.M. Bourke, D.C. Dunand, E. Ustundag, Appl. Phys. A: Mater. Sci. Process 74 (2002) S1707–S1709.
[9] A.D. Krawitz, T.M. Holden, MRS Bull. 15 (11) (1990) 57–64.
[10] S. Majumdar, J.P. Singh, D. Kupperman, A.D. Krawitz, J. Eng. Mater. Technol. Trans. ASME 113 (1) (1991) 51–59.
[11] A.D. Krawitz, J. Met. 39 (10) (1987) 27.
[12] M.A.M. Bourke, J.A. Goldstone, R.A. Robinson, Physica B 213 (1995) 806–808.
[13] M. Lee, R.S. Gilmore, J. Mater. Sci. 17 (1982) 2657–2660.
[14] M.A.M. Bourke, D.C. Dunand, E. Ustundag, Appl. Phys. A 74 (2002) S1707–S1709.
[15] A.D. Krawitz, R.A. Winholtz, C.M. Weisbrook, Mater. Sci. Eng. A 206 (1996) 176–182.
[16] C.M. Weisbrook, A.D. Krawitz, Mater. Sci. Eng. A 209 (1996) 318–329.
[17] G.E. Bacon, Neutron Diffraction, third ed., Clarendon Press, Oxford, 1975, p. 43.
[18] L.F. Smith, A.D. Krawitz, P. Clarke, S. Saimoto, N. Shi, R.J. Arsenault, Mater. Sci. Eng. A 159 (2) (1992) L13–L15.
[19] M.R. Daymond, P.J. Withers, Mater. Sci. Technol. 11 (3) (1995) 228–235.
[20] D.H. Carter, M.A.M. Bourke, Acta Mater. 48 (2000) 2885–2900.
[21] ABAQUS Users Manual, Version 6.3, HKS, 2003.
[22] A.D. Krawitz, D.G. Reichel, R. Hitterman, Mater. Sci. Eng. A 119 (1989) 127–134.
[23] G.S. Upadhyaya, Cemented Tungsten Carbides, Noyes Publications, Westwood, 1998.
[24] Y. Mishima, S. Ochiai, N. Hamao, M. Yodogawa, T. Suzuki, Trans. Jpn. Inst. Met. 27 (1986) 656–664.
[25] B. Roebuck, E.A. Almond, A.M. Cottenden, Mater. Sci. Eng. 66 (1984) 179–194.
[26] C.M. Weisbrook, V.S. Gopalaratnam, A.D. Krawitz, Mater. Sci. Eng. A 201 (1995) 134–142.
[27] E.F. Drake, A.D. Krawitz, Metall. Trans. A 12A (1981) 505–513.
[28] K. Seol, A.D. Krawitz, Mater. Sci. Eng. A 127 (1990) 1–5.